PHYSICAL REVIEW D **95,** 115009 (2017)

Searches for new physics at the Hyper-Kamiokande experiment

Kevin J. Kelly
Northwestern University, Department of Physics and Astronomy,
2145 Sheridan Road, Evanston, Illinois 60208, USA
(Received 23 March 2017; published 8 June 2017)

We investigate the ability of the upcoming Hyper-Kamiokande (Hyper-K) neutrino experiment to detect new physics phenomena beyond the standard, three-massive-neutrinos paradigm; namely, the existence of a fourth, sterile neutrino or weaker-than-weak, nonstandard neutrino interactions. With both beam-based neutrinos from the Japan Proton Accelerator Research Complex (J-PARC) and atmospheric neutrinos, Hyper-K is capable of exploring new ranges of parameter space in these new-physics scenarios. We find that Hyper-K has comparable capability to the upcoming Deep Underground Neutrino Experiment (DUNE), and that combining both beam- and atmospheric-based data can clear up degeneracies in the parameter spaces of interest. We also comment on the potential improvement in searches for new physics if a combined analysis were performed using Hyper-K and DUNE data.

DOI: 10.1103/PhysRevD.95.115009

I. INTRODUCTION

With the discovery that neutrinos have mass and leptons mix, neutrino oscillations have been identified as a clear direction to study physics beyond the Standard Model (SM). Many existing experiments have measured the neutrino mass splittings and the leptonic mixing matrix, and several next-generation experiments, such as the Hyper-Kamiokande Experiment (Hyper-K) [1,2] and the Deep Underground Neutrino Experiment (DUNE) [3,4], have been proposed to continue this study at long baselines. Hyper-K and DUNE aim to answer several remaining questions regarding lepton mixing with three SM neutrinos that have mass (which we will refer to as the "three-massive-neutrinos paradigm"). In addition to this, the next generation experiments will be able to test for physics beyond the three-massive-neutrinos paradigm.

Many hypotheses exist that extend beyond the three-massive-neutrinos paradigm that are still consistent with present data. Among these are the proposal that the leptonic mixing matrix is nonunitary (unlike the quark mixing matrix, the unitarity of the leptonic mixing matrix is not well-constrained [5–7]), the existence of singlet fermion fields propagating in large extra dimensions, the addition of a fourth neutrino state, and the existence of interactions involving neutrinos aside from the weak interactions. In this work, we will focus on the last two, referred to, respectively, as the sterile neutrino and nonstandard neutrino interaction hypotheses.

The addition of a fourth, sterile neutrino as an extension to the three-massive-neutrinos paradigm has been studied extensively in the literature—theoretical motivations for a fourth neutrino are wide ranging, from explaining the mechanism by which the light neutrinos acquire a mass (see, e.g., Ref. [8]), to alleviating experimental oscillation results that appear inconsistent with the three-massive-neutrinos paradigm [9–14]. These motivations require a fourth neutrino with widely varying mass—in this work, we will focus on cases with a new mass eigenstate $m_4 \lesssim 1$ eV, which can impact neutrino oscillations at long baselines. Sterile neutrinos in this mass range have been studied in the context of short-baseline oscillations in Refs. [15–19], and Refs. [17,18,20–34] have studied the impact of a sterile neutrino in long-baseline oscillations, as this work will. Constraints on a fourth neutrino over a wider range of masses have been discussed in Refs. [30,35–39].

Nonstandard neutrino interactions (NSI), originally proposed as a solution to the solar neutrino problem [40], have been studied in a number of situations, all of which introduce additional interactions involving neutrinos and other fermions. References [41–47] have studied the impact of NSI on solar neutrino oscillations, Refs. [48–61] have studied how they contribute to atmospheric neutrino oscillations, and Refs. [34,62–90] have studied NSI in the context of accelerator-based neutrino oscillations, particularly focusing on the upcoming long-baseline oscillation experiments. Recently, NSI have been discussed regarding the Hyper-Kamiokande experiment in Refs. [74,91–96]. This work adds to the discussion of NSI at Hyper-K by conducting a thorough, multiparameter analysis of the sensitivity of the experiment, utilizing both its beam- and atmospheric-based capabilities.

This manuscript is organized as follows: in Sec. II, we introduce the oscillation formalism used when discussing the three-massive-neutrinos paradigm, as well as the extensions to this: sterile neutrinos and nonstandard neutrino interactions. In Sec. III, we discuss the capabilities of the Hyper-Kamiokande experiment, in both the detection of neutrinos generated from the Japan Proton Accelerator Research Complex (J-PARC) and the detection of neutrinos produced in the atmosphere. Here, we also discuss our analysis method. In Sec. IV, we present the results of our analyses, including the ability of the Hyper-Kamiokande

 © 2017 American Physical Society

experiment to detect sterile neutrinos and nonstandard interactions, and in Sec. V, we offer some concluding remarks.

II. OSCILLATIONS AND NEW NEUTRINO PHYSICS

We direct the reader to, for example, Refs. [26,73] for more thorough discussions on long-baseline neutrino oscillations regarding four-neutrino scenarios and nonstandard neutrino interactions (NSI), respectively. Here, we explain the three-massive-neutrinos paradigm and three-neutrino oscillations, and in Secs. II A and II B, we introduce the formalisms regarding oscillations with four neutrinos and with NSI, respectively.

With three neutrinos and two nonzero mass-squared splittings $\Delta m^2_{ij} \equiv m^2_j - m^2_i$, we characterize oscillations using a 3×3 unitary, PMNS matrix U. This requires three mixing angles (θ_{12}, θ_{13}, and θ_{23}) and one CP-violating phase (δ) to describe oscillations. We use the particle data group convention for U [97]. The mixing angles and mass splittings have been measured to be nonzero, but two important measurements remain: the value of δ and the mass hierarchy, whether $\Delta m^2_{13} > 0$ (normal hierarchy) or $\Delta m^2_{13} < 0$ (inverted hierarchy).

With neutrino states in the flavor basis (e, μ, τ), the probability for a neutrino of flavor α to propagate a distance L and be detected as flavor β is denoted by the amplitude mod-squared

$$P_{\alpha\beta} \equiv |\mathcal{A}_{\alpha\beta}|^2 = |\langle \nu_\beta | U e^{-iH_{ij}L} U^\dagger | \nu_\alpha \rangle|^2, \qquad (2.1)$$

where U is the PMNS matrix and H_{ij} is the Hamiltonian in the basis in which propagation in vacuum is diagonal. This equation is only valid when the Hamiltonian is constant over the entire distance L, and while the neutrinos remain a coherent superposition of plane waves. In this basis and in the ultrarelativistic approximation, $H_{ij} \equiv 1/(2E_\nu)$ diag$\{0, \Delta m^2_{12}, \Delta m^2_{13}\}$, where E_ν is the neutrino energy. While propagating through earth, interactions between the neutrinos and the electrons, protons, and neutrons introduce an effective interaction potential V. As these interactions are mediated by $W-$ and $Z-$ bosons (the same interactions that govern neutrino production and detection), V is diagonal in the flavor basis. With this effective interaction potential, we must augment the propagation Hamiltonian,

$$H_{ij} \to H_{ij} + U^\dagger_{i\alpha} V_{\alpha\beta} U_{\beta j}, \qquad (2.2)$$

where the PMNS matrix is used to rotate the potential into the mass basis. The interactions with protons and neutrons are identical between ν_α, $\alpha = e, \mu, \tau$, and can be absorbed as a phase in the Hamiltonian. The remaining term, coming from t-channel interaction between a ν_e and an electron, mediated by a W-boson, is $V_{\alpha\beta} = A$ diag $\{1, 0, 0\}$, where $A = \sqrt{2} G_F n_e$. G_F is the Fermi constant, and n_e is the number density of electrons along the path of propagation. For antineutrinos oscillating, $U \to U^*$ and $A \to -A$ (to account for the s-channel interaction of $\bar{\nu}_e$ with e^- in matter).

Equation (2.1) is only valid for an interaction potential $V_{\alpha\beta}$ that is constant over the entire baseline length L. For propagation through the earth, the path length and matter density depend strongly on the zenith angle θ_z. We simulate the density profile of the earth to be piecewise constant with four distinct regions ranging from 3 g/cm^3 to 13 g/cm^3, closely resembling the preliminary reference earth model (PREM) earth density model [98]. Equation (2.1) is then modified, becoming

$$P_{\alpha\beta} = |\mathcal{A}_{\alpha\beta}|^2 = \left| \langle \nu_\beta | U \left(\prod_{n=1}^{N} e^{-iH^{(n)}_{ij} L_n} \right) U^\dagger | \nu_\alpha \rangle \right|^2, \qquad (2.3)$$

where N is the number of distinct regions through which a chord along angle θ_z passes, $H^{(n)}_{ij}$ is the mass-basis Hamiltonian with the matter density of region n, and L_n is the length of the chord through this region.

Unless otherwise specified, we will use the results of the most recent NuFIT calculations (Ref. [99]) as physical values for three-neutrino parameters. These values are listed in Table I. We assume that there is a normal mass hierarchy and do not marginalize over the hierarchy in our analysis. This assumption relies on the measurement of the neutrino mass hierarchy before Hyper-K begins collecting data.

A. Sterile neutrino

While the three-massive-neutrinos paradigm is in agreement with nearly all existing oscillation data, several hints exist that might be explained by a fourth neutrino and a mass splitting of $\Delta m^2_{14} \simeq 1$ eV^2 [9–14]. Mass splittings in this range are best probed by oscillation experiments with baseline lengths and neutrino energies that satisfy $L/E_\nu \simeq 1$ km/GeV. As they are designed to measure Δm^2_{13}, long-baseline experiments such as Hyper-K and DUNE are sensitive to lower mass splittings ($\Delta m^2_{14} \simeq 10^{-2}$ eV^2). They also provide a complementary probe to the short-baseline experiments' searches for eV^2-scale splittings.

In order to accommodate a fourth neutrino, we must extend the $U(3)$ PMNS matrix into a $U(4)$ matrix. In doing so, we require six mixing angles (ϕ_{ij}; $i < j$; $i, j = 1, 2, 3, 4$) and three CP-violating phases (η_i; $i = 1, 2, 3$).[1] Assuming unitarity, the relevant matrix elements are

[1]We explicitly label the mixing angles ϕ_{ij} and phases η_i in the four-neutrino scenario to reduce confusion with the three-massive-neutrinos paradigm. In the limit that $\phi_{i4} \to 0$, $\phi_{12,13,23} = \theta_{12,13,23}$ and the phase $\eta_1 = \delta$.

TABLE I. Input values assumed for three-neutrino parameters as extracted from the NuFIT Collaboration, Ref. [99]. One-sigma ranges are quoted for Δm^2_{12} and $|U_{e2}|^2$ (calculated from measurements of $\sin^2\theta_{12}$ and $\sin^2\theta_{13}$), which are used as priors in later sections.

Parameter	$\sin^2\theta_{12}$	$\sin^2\theta_{23}$	$\sin^2\theta_{13}$	δ	Δm^2_{12}	Δm^2_{13}	$\lvert U_{e2}\rvert^2$
Value	0.306	0.441	0.02166	-1.728	$(7.50^{+0.19}_{-0.17})\times 10^{-5}$ eV^2	2.524×10^{-3} eV^2	0.2994 ± 0.0117

$$U_{e2} = s_{12}c_{13}c_{14}, \tag{2.4}$$

$$U_{e3} = s_{13}c_{14}e^{-i\eta_1}, \tag{2.5}$$

$$U_{e4} = s_{14}e^{-i\eta_2}, \tag{2.6}$$

$$U_{\mu 2} = c_{24}(c_{12}c_{23} - e^{i\eta_1}s_{12}s_{13}s_{23}) - e^{i(\eta_2-\eta_3)}s_{12}c_{13}s_{14}s_{24}, \tag{2.7}$$

$$U_{\mu 3} = s_{23}c_{13}c_{24} - e^{i(\eta_2-\eta_3-\eta_1)}s_{13}s_{14}s_{24}, \tag{2.8}$$

$$U_{\mu 4} = s_{24}c_{14}e^{-i\eta_3}, \tag{2.9}$$

$$U_{\tau 2} = c_{34}(-c_{12}s_{23} - e^{i\eta_1}s_{12}s_{13}c_{23}) - e^{i\eta_2}c_{13}s_{12}c_{24}s_{14}s_{34} - e^{i\eta_3}(c_{12}c_{23} - e^{i\eta_1}s_{12}s_{13}s_{23})s_{24}s_{34}, \tag{2.10}$$

$$U_{\tau 3} = c_{13}c_{23}c_{34} - e^{i(\eta_2-\eta_1)}s_{13}c_{24}s_{14}s_{34} - e^{i\eta_3}s_{23}c_{13}s_{24}s_{34}, \tag{2.11}$$

$$U_{\tau 4} = c_{14}c_{24}s_{34}, \tag{2.12}$$

where $s_{ij} \equiv \sin\phi_{ij}$ and $c_{ij} \equiv \cos\phi_{ij}$. The remaining matrix elements may be determined by the unitarity of U.

As with the PMNS matrix, the propagation Hamiltonian must be extended. The Hamiltonian in vacuum becomes $H_{ij} = 1/(2E_\nu)\,\mathrm{diag}\{0, \Delta m^2_{12}, \Delta m^2_{13}, \Delta m^2_{14}\}$, and the interaction potential for a constant-density environment becomes

$$V_{\alpha\beta} \to A\begin{pmatrix} 1 & 0 & 0 & 0 \\ 0 & 0 & 0 & 0 \\ 0 & 0 & 0 & 0 \\ 0 & 0 & 0 & \frac{n_n}{2n_e} \end{pmatrix}, \tag{2.13}$$

where n_n is the number density of neutrons, which we assume to be equal to the number density of electrons in Earth. This term comes from the phase removed from the potential discussed above, along with the assumption that the additional eigenstate in the flavor basis is sterile and does not interact with the $W-$ or $Z-$ bosons.

As an illustrative example of a sterile neutrino hypothesis, we use the parameters shown in Table II for comparisons in figures. These parameters are chosen to highlight differences in oscillation probabilities and event yields, and are not used in any of the analyses discussed in Sec. IV. We will be interested in the oscillation channels $P_{\mu\mu}$ and $P_{\mu e}$ (and their CP conjugates) for this work. While $P_{\mu\mu}$ is sensitive predominantly to the value of $\sin^2\phi_{24}$, $P_{\mu e}$ is most sensitive to the parameter $\sin^2(2\phi_{e\mu}) \equiv \sin^2(2\phi_{14})\sin^2\phi_{24} = 4|U_{e4}|^2|U_{\mu 4}|^2$. This is the free parameter seen most often in sterile neutrino searches at short baselines, measuring $P_{\mu e}$ or $P_{e\mu}$. Constraints on the remaining parameter space come from reactor neutrino experiments measuring P_{ee} and $P_{\bar{e}\bar{e}}$, sensitive to $\sin^2\phi_{14}$.

B. Nonstandard neutrino interactions (NSI)

We consider the following dimension-six four fermion operator mediating nonstandard neutrino interactions:

$$\mathcal{L}_{\mathrm{NSI}} = -2\sqrt{2}G_F(\bar{\nu}_\alpha\gamma_\rho\nu_\beta)(\epsilon^{f\tilde{f}L}_{\alpha\beta}\bar{f}_L\gamma^\rho\tilde{f}_L + \epsilon^{f\tilde{f}R}_{\alpha\beta}\bar{f}_R\gamma^\rho\tilde{f}_R) + \mathrm{H.c.}, \tag{2.14}$$

where G_F is the Fermi constant and $\epsilon_{\alpha\beta}$ represent the strength, relative to the weak interactions, of NSI between neutrinos of flavor α and β with fermions f and $\tilde{f}$ of chirality s. As is standard (see, e.g., Refs. [43,52–55,57,62,73,100,101]), we make several assumptions:

(i) $f = \tilde{f} = e, u, d$—we only consider diagonal, neutral current interactions with charged, first-generation fermions.

(ii) We only consider NSI effects during propagation. For a recent investigation of source, detector, and propagation effects in a long-baseline context, see Ref. [85].

(iii) For propagation through earth, we define $\epsilon_{\alpha\beta} \equiv \sum_f \epsilon^f_{\alpha\beta} n_f/n_e$, with $\epsilon^f_{\alpha\beta} \equiv \epsilon^{ffL}_{\alpha\beta} + \epsilon^{ffR}_{\alpha\beta}$ and n_f the number density of fermion f. We also assume that $n_u = n_d = 3n_e$.

TABLE II. Input values used for an illustrative sterile neutrino hypothesis for comparisons in figures throughout this work. The unlisted parameters $\sin^2\phi_{ij}$ are equal to the values $\sin^2\theta_{ij}$ in Table I for $i, j = 1, 2, 3$, and η_1 is equal to the value of δ in Table I.

Parameter	$\sin^2(2\phi_{14})$	$\sin^2\phi_{24}$	$\sin^2\phi_{34}$	Δm^2_{14}	η_2	η_3
Value	5×10^{-2}	2×10^{-2}	0	6×10^{-3} eV^2	0	0

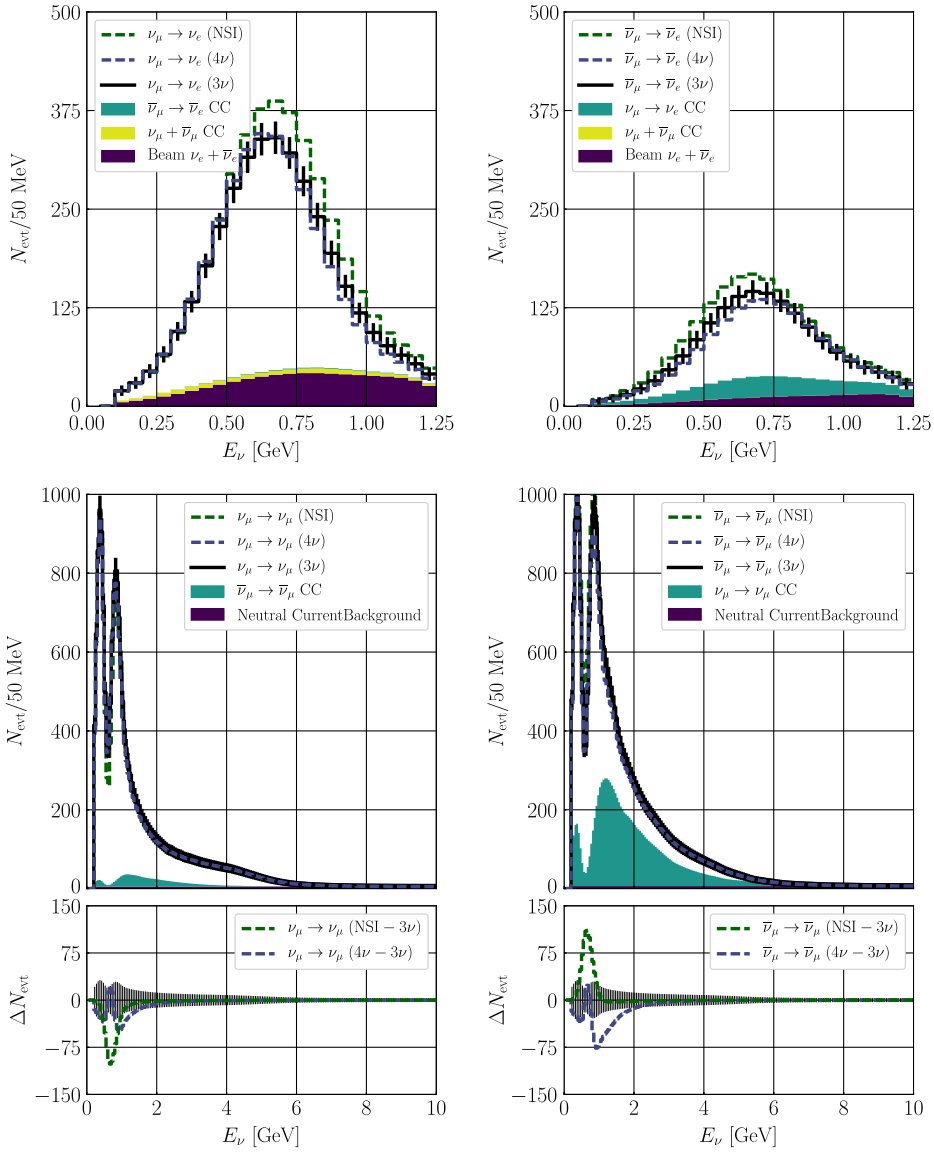

FIG. 1. Expected yields in the appearance channels (top) and disappearance channels (middle) assuming ten years of data collection at the Hyper-Kamiokande experiment with a ratio of 1 : 3 for the duration of neutrino and antineutrino modes. The left panels display yields during neutrino mode, and the right panels display yields during antineutrino mode. In each panel, backgrounds are displayed as a stacked histogram, with opposite-sign signal events shown in teal, muon-neutrino misidentification shown in yellow in the appearance channels, beam contamination backgrounds in purple in the appearance channels, and neutral current backgrounds in purple in the disappearance channels. As discussed in the text, expected neutral current event rates have been included by inflating the beam contamination background for the appearance channels, and as a flat background in the disappearance channels. Three different sets of overall signal plus background yields are shown in each panel: for a three-neutrino scenario assuming parameters from Table I (black, including statistical error bars), a four-neutrino scenario assuming parameters from Table II (blue, dashed), and a nonstandard interaction scenario assuming parameters from Table III (green, dashed). The bottom panels additionally show differences in the number of expected events per bin between the NSI and three-neutrino scenarios (green) and four- and three-neutrino scenarios (blue).

With NSI, the interaction potential for a constant-density region is modified,

$$V_{\alpha\beta} \to A \begin{pmatrix} 1+\epsilon_{ee} & \epsilon_{e\mu} & \epsilon_{e\tau} \\ \epsilon_{e\mu}^* & \epsilon_{\mu\mu} & \epsilon_{\mu\tau} \\ \epsilon_{e\tau}^* & \epsilon_{\mu\tau}^* & \epsilon_{\tau\tau} \end{pmatrix}. \tag{2.15}$$

In general, the addition of NSI amounts to nine new parameters, as the off diagonal elements of $V_{\alpha\beta}$ are complex. Since one element proportional to the identity may be absorbed as a phase in oscillations, we redefine $V'_{\alpha\beta} = V_{\alpha\beta} - \epsilon_{\mu\mu}\mathbb{1}$. When considering antineutrino oscillations, $A \to -A$ (as in the three-neutrino hypothesis) and $\epsilon_{\alpha\beta} \to \epsilon_{\alpha\beta}^*$.

As with the sterile neutrino hypothesis, we give a set of illustrative NSI parameters for comparison against the three-neutrino hypothesis in figures. For a thorough discussion of the bounds on NSI parameters for neutrino propagation through the Earth, we refer the reader to Refs. [100,102,103].

III. THE HYPER-KAMIOKANDE EXPERIMENT

The Hyper-Kamiokande (Hyper-K) Experiment is a proposed next-generation neutrino experiment that utilizes two water Cerenkov detectors with total mass of 0.99 megatons (0.56 Mton fiducial) located in the Tochibora Mine, 8 km south of the existing Super-Kamiokande (Super-K) experiment [1]. The upgraded Japan Proton Accelerator Research Complex (J-PARC) proton synchrotron beam is expected to deliver 1.56×10^{22} protons on target over ten years of data collection. In Sec. III A, we discuss the capability of Hyper-K using the neutrino beam originating at J-PARC, 295 km away from the detector, and in Sec. III B, we discuss the capability of Hyper-K in utilizing atmospheric neutrinos. A recent proposal (see Ref. [2]) suggests placing one detector in Korea for a longer baseline; however, we consider only the original proposal. References [92,94,96] discuss the potential of this setup in light of NSI.

A. Beam-based detector capabilities

The J-PARC beam is capable of operating in two modes, neutrino and antineutrino, in which the dominant contributions to the beam are ν_μ and $\bar{\nu}_\mu$, respectively. Reference [1] has determined that the optimal ratio for operating in these two modes is $1:3$ for $\nu:\bar{\nu}$, and so we take this, and an assumption of ten years of data collection, for our analysis. The two analyses performed are the appearance ($\nu_\mu \to \nu_e$) and disappearance ($\nu_\mu \to \nu_\mu$) channels. Both channels assume bins of 50 MeV, and we smear[2] the reconstructed energy distributions attempting to match the results of Ref. [1]. Electron (appearance) candidates range in energy between 100 MeV and 1.25 GeV, where muon (disappearance) candidates range between 200 MeV and 10 GeV. Using projected fluxes from Ref. [1], neutrino-nucleon cross sections from Ref. [104], and oscillation probabilities calculated given a particular hypothesis, we determine the expected event yield at Hyper-K assuming ten years of data collection with a ratio of $1:3$ for $\nu:\bar{\nu}$ modes.

[2]This smearing and our attempted replication of reconstruction efficiencies lead to apparent discrepancies between our simulation and that of Ref. [1], where our distributions appear more smeared, particularly, in the disappearance channels. We find that changing the smearing has little-to-no impact on the results of this work, as long as the signal and background rates are normalized to those presented in Ref. [1].

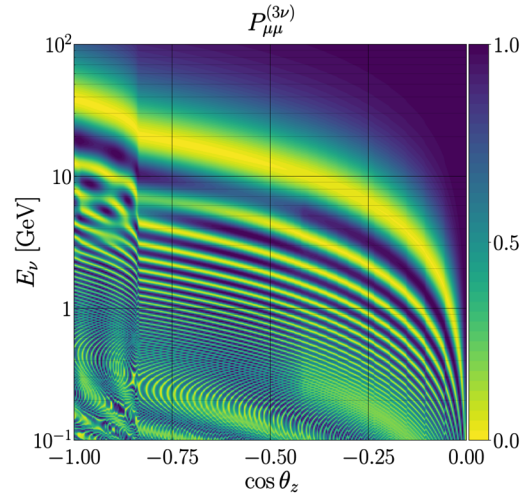

FIG. 2. Oscillation plot of $P_{\mu\mu}$ assuming three neutrinos exist with parameters in Table I as a function of $\cos\theta_z$, where θ_z is the zenith angle (with $\theta_z = 0$ being directly overhead) and neutrino energy E_ν. Here, we assume a piecewise-constant density profile for the Earth so that Eq. (2.3) may be utilized. For comparison against previous works (see, e.g., Ref. [105]), we display only $\cos\theta_z \in [-1, 0]$ and find that our results match those using a more sophisticated density profile like PREM [98]. We calculate probabilities over the entire range of θ_z in practice.

Figure 1 displays expected event yields at Hyper-K assuming ten years of data collection. The top panels display appearance channels for ν mode (left) and $\bar{\nu}$ mode (right), and the bottom panels display disappearance channels for ν mode (left) and $\bar{\nu}$ mode (right). For appearance channels, we consider background contributions due to opposite sign signal ("$\bar{\nu}_\mu \to \bar{\nu}_e$ CC" and "$\nu_\mu \to \nu_e$ CC", teal), unoscillated muon contamination ("$\nu_\mu + \bar{\nu}_\mu$ CC", yellow), and unoscillated electron contamination ("beam $\nu_e + \bar{\nu}_e$", purple). As we do not have strong information regarding the neutral current backgrounds, we have inflated the unoscillated electron contamination to match background rates in Ref. [1]. For disappearance channels, we include opposite sign signal ("$\bar{\nu}_\mu \to \bar{\nu}_\mu$ CC" and "$\nu_\mu \to \nu_\mu$ CC", teal) and a flat neutral current background (purple). For each panel, we display total yields assuming three neutrinos exist (using the parameters in Table I, black, with statistical error bars shown), assuming four neutrinos exist (using the illustrative case in Table II, blue), and assuming NSI (using the illustrative case in Table III, green).

TABLE III. Input values used for an illustrative NSI hypothesis for comparisons in figures throughout this work. Three-neutrino parameters are equal to their values in Table I. We include a star on the value of $\epsilon_{\mu\mu}$ as a reminder that this parameter is set to zero in our analysis, as discussed in the text.

Parameter	ϵ_{ee}	$\epsilon_{e\mu}$	$\epsilon_{e\tau}$	$\epsilon_{\mu\mu}$	$\epsilon_{\mu\tau}$	$\epsilon_{\tau\tau}$
Value	0	$0.5e^{i\pi/3}$	$0.5e^{-i\pi/4}$	$0\star$	0	-1

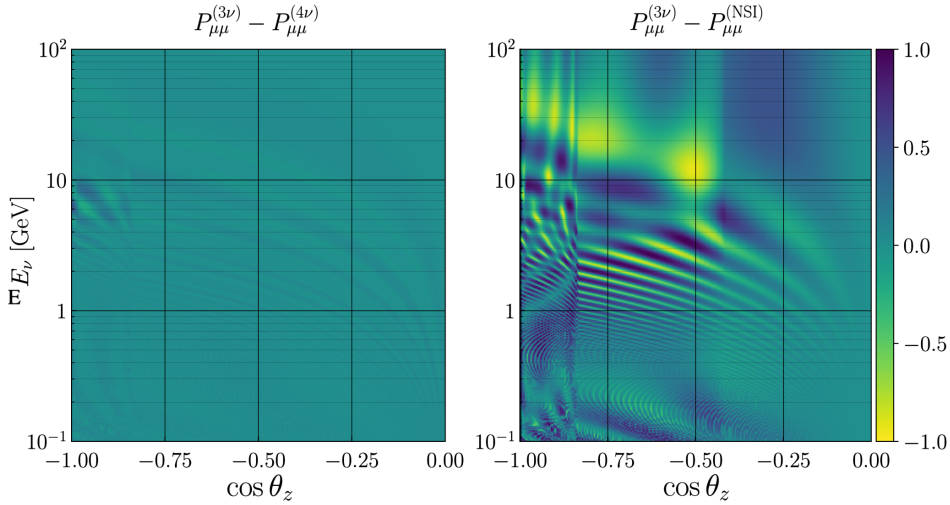

FIG. 3. Differences in the oscillation probability $P_{\mu\mu}$ with the three neutrino case shown in Fig. 2 for a four-neutrino scenario with parameters from Table II (left) and an NSI scenario with parameters from Table III (right).

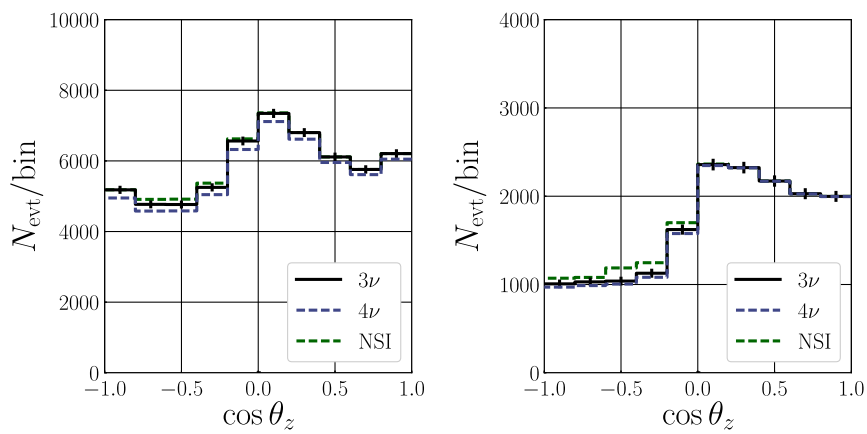

FIG. 4. Expected muon-type event yields at Hyper-Kamiokande assuming a three-neutrino scenario with parameters from Table I (black, including statistical error bars), assuming a four-neutrino scenario with parameters from Table II (blue, dashed), and assuming NSI exist with parameters from Table III (green, dashed). Oscillation probabilities are calculated as discussed in the text, and then convolved with fluxes from Ref. [106]. The event distribution is divided into low-energy ($E_\nu < 1.3$ GeV, left) and high-energy ($E_\nu > 1.3$ GeV, right) samples, and smeared by 10° (5°) for the low- (high-) energy distribution due to the correlation between the incident muon neutrino and outgoing muon tracks. Distributions are then binned in ten bins of $\cos\theta_z$, as seen in the figure.

B. Atmospheric-based detector capabilities

In addition to neutrinos produced by the J-PARC beam, Hyper-K is sensitive to atmospheric neutrinos, similar to its predecessor Super-K. The dominant channel contributing to atmospheric neutrino oscillations at Hyper-K is $P_{\mu\mu}$. Figure 2 displays an oscillogram of $P_{\mu\mu}$ for a three-neutrino case as a function of the (cosine of the) zenith angle and neutrino energy. Additionally, we show differences in oscillation probability in Fig. 3 between a three-neutrino case and an four-neutrino case (left) and between a three-neutrino case and an NSI case (right). While the figures here only display the range $\cos\theta_z \in [-1, 0]$ (upward-going neutrinos) for the sake of comparison, the entire range of zenith angles is calculated in practice. Despite using a piecewise-constant density profile, the behavior here matches that seen in Ref. [105].

Reference [106] details the expected atmospheric neutrino flux at the location of Super-K, and we estimate the yield after ten years at Hyper-K by increasing the Super-K exposure by a factor of 20. We only consider measurements of muon-type neutrinos in the detector—this relies on the muon (anti)neutrino flux in the upper atmosphere multiplied by $P_{\mu\mu}$ ($P_{\bar{\mu}\bar{\mu}}$) and the electron (anti) neutrino flux multiplied by $P_{e\mu}$ ($P_{\bar{e}\bar{\mu}}$). Considering appearance of electron- and tau-type neutrinos would improve results by measuring the oscillation probabilities $P_{\mu e}$, $P_{\mu\tau}$, etc., however we analyze only muon-type

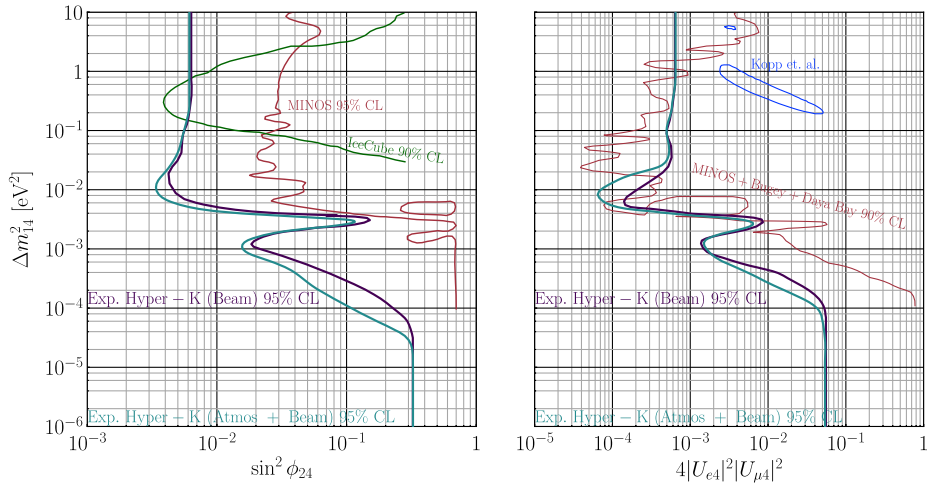

FIG. 5. Expected sensitivity to a fourth neutrino assuming ten years of only beam-based data at Hyper-Kamiokande at 95% C.L. (purple) and including atmospheric-based data (teal). Regions above and to the right of these curves will be excluded at 95% C.L. by Hyper-K if only three neutrinos exist. The left panel displays sensitivity in the $\sin^2\phi_{24}$—Δm^2_{14} plane, with contributions predominantly from the disappearance channels, and the right panel displays sensitivity in the $4|U_{e4}|^2|U_{\mu4}|^2 = 4\sin^2\phi_{14}\sin^2\phi_{24}\cos^2\phi_{14}$—$\Delta m^2_{14}$ plane, with contributions predominantly from the appearance channels. All unseen parameters are marginalized in each panel. In the left panel, we display existing bounds from the MINOS [108] (red, 95% C.L.) and IceCube [109] (green, 90% C.L.) experiments. In the right panel, we display the most competitive existing bound in this parameter space, a combined analysis from the MINOS, Bugey, and Daya Bay experiments [110] (red, 90% C.L.) and the preferred parameter space of various reactor and short-baseline sterile neutrino hints from a combined global analysis in Ref. [111] (blue). Gaussian priors are included on the values of $|U_{e2}|^2 = 0.2994 \pm 0.0117$ and $\Delta m^2_{12} = (7.50 \pm 0.18) \times 10^{-5}$ eV^2. Estimated sensitives are calculated utilizing EMCEE [107].

neutrino measurements for simplicity. As with Super-K, we divide up muon neutrino samples into sub-GeV ($E_\nu < 1.3$ GeV) and multi-GeV events, and we divide up the incoming direction of the neutrinos (the zenith angle θ_z) into ten bins of $\cos\theta_z$. Additionally, we smear the reconstructed low- (high-) energy distribution by 10° (5°) given the correlation between the incident muon neutrino and outgoing muon track. Expected event counts as a function of $\cos\theta_z$ after smearing and binning are shown in Fig. 4. Comparing Figs. 3 and 4, we see that, for the majority of energies, $P^{(4\nu)}_{\mu\mu} < P^{(3\nu)}_{\mu\mu}$, leading to fewer expected events in Fig. 4. Also, we see that, predominantly for higher energy neutrinos ($E_\nu \gtrsim 1$ GeV), $P^{(\mathrm{NSI})}_{\mu\mu} > P^{(3\nu)}_{\mu\mu}$, leading to a higher number of expected events in the right panel of Fig. 4.

C. Analysis method

Our analysis method is as follows. First, we simulate expected yields for beam-based and atmospheric neutrino detection assuming three neutrinos exist, with parameters shown in Table I. Then, given a test hypothesis with parameters[3] $\vec{\vartheta}$, we calculate a chi-squared function. Included in the chi-squared function are Gaussian priors on the solar mass splitting[4] Δm^2_{12} and $|U_{e2}|^2$, where the one-sigma ranges are given in Table I. We also include normalization uncertainties in the chi-squared function: 5% signal and background uncertainties for the beam-based data, and 10% for the atmospheric-based data. While certain parameters ($\sin^2\phi_{34}, \eta_{2,3}$ for the sterile neutrino hypothesis, and ϵ_{ee} and $\epsilon_{\mu\tau}$ for the NSI hypothesis) were set to zero for the illustrative examples listed in Tables II and III, none of the parameters (except $\epsilon_{\mu\mu}$ as discussed above) are fixed in our analysis. This amounts to 12 free parameters for the sterile neutrino scenario and 14 for the NSI scenario.

We then use the Markov chain Monte Carlo package EMCEE to calculate posterior likelihood distributions in the parameter space of a particular test hypothesis, and from these, we calculate one- and two-dimensional chi-squared distributions, marginalized over all other parameters [107]. We define the 95% (99%) C.L. sensitivity reach of Hyper-K as regions where $\chi^2 - \chi^2_{\mathrm{min}} > 5.99$ (9.21) for two-dimensional figures and $\chi^2 - \chi^2_{\mathrm{min}} > 3.84$ (6.63) for one-dimensional figures. For each new physics hypothesis, we perform this analysis using only beam-based results, and using a combination of beam- and atmospheric-based results.

[3]For the sterile neutrino hypothesis, we use the parameter space $\vec{\vartheta} = (\phi_{12}, \phi_{13}, \phi_{23}, \Delta m^2_{12}, \Delta m^2_{13}, \eta_1, \sin^2\phi_{24}, 4|U_{e4}|^2|U_{\mu4}|^4, \sin^2\phi_{34}, \eta_2, \eta_3, \Delta m^2_{14})$, where we use $4|U_{e4}|^2|U_{\mu4}|^2 = 4\sin^2\phi_{14}\cos^2\phi_{14}\sin^2\phi_{24}$ as an independent parameter to compare against short-baseline sterile neutrino searches.

[4]The one-sigma range on Δm^2_{12} in Table I is nearly symmetric—we approximate the one-sigma range to be $\Delta m^2_{12}(7.50 \pm 0.18) \times 10^{-5}$ eV^2 in our analysis.

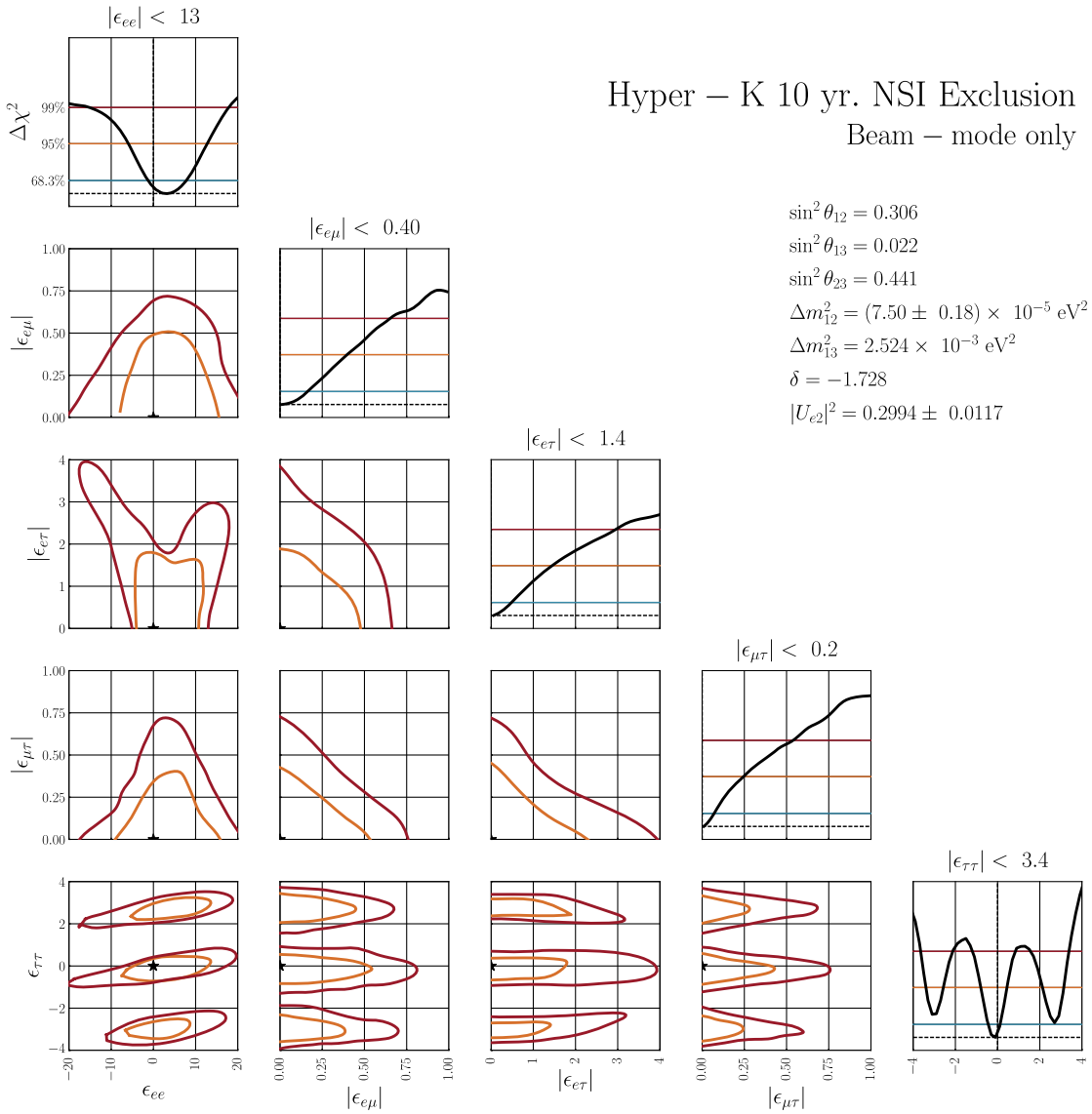

FIG. 6. Expected sensitivity to nonzero NSI assuming ten years of beam-based data collection at Hyper-Kamiokande at 95% C.L. (orange) and 99% C.L. (red). In each panel, all unseen parameters, including three-neutrino parameters and phases of off diagonal NSI, are marginalized. The top panel of each column displays expected one-dimensional $\Delta\chi^2$ sensitivity for each parameter, including horizontal lines displaying 68.3% (blue), 95% (orange), and 99% (red) C.L. Above each column, the expected limits at 95% C.L. for each parameter are shown. Gaussian priors are included on the values of $|U_{e2}|^2 = 0.2994 \pm 0.0117$ and $\Delta m^2_{12} = (7.50 \pm 0.18) \times 10^{-5}$ eV^2. Estimated sensitivities are calculated utilizing EMCEE [107].

IV. RESULTS

A. Sterile neutrino

Here, we generate data consistent with only three neutrinos existing and analyze the sensitivity of the Hyper-K experiment to detect a fourth neutrino. Figure 5 displays the sensitivity reach of the Hyper-K experiment in the $\sin^2\phi_{24}$—Δm^2_{14} (left) and $4|U_{e4}|^2|U_{\mu4}|^2$—Δm^2_{14} (right) planes using only data from the beam-based capabilities (purple). The region above and to the right of each curve will be excluded at 95% C.L. by Hyper-K if only three neutrinos exist. In both panels, we see that in the high-Δm^2_{14} range, oscillations average out, and in the low-Δm^2_{14} range, while oscillations due to the fourth mass eigenstate are not detectable, nonzero mixing angles ϕ_{i4} can impact the unitarity of the 3×3 submatrix of the 4×4 PMNS matrix and may be detectable at Hyper-K. This feature has been discussed in the context of long-baseline neutrino oscillations (at DUNE) previously in Ref. [26]. We also see a feature in both panels of Fig. 5 where sensitivity is weaker for $\Delta m^2_{14} \sim 10^{-3}$–$10^{-2}$ eV^2. This comes from the fact that Δm^2_{13} is in this range, and there is degeneracy between the mixing angles ϕ_{i4} and ϕ_{i3}.

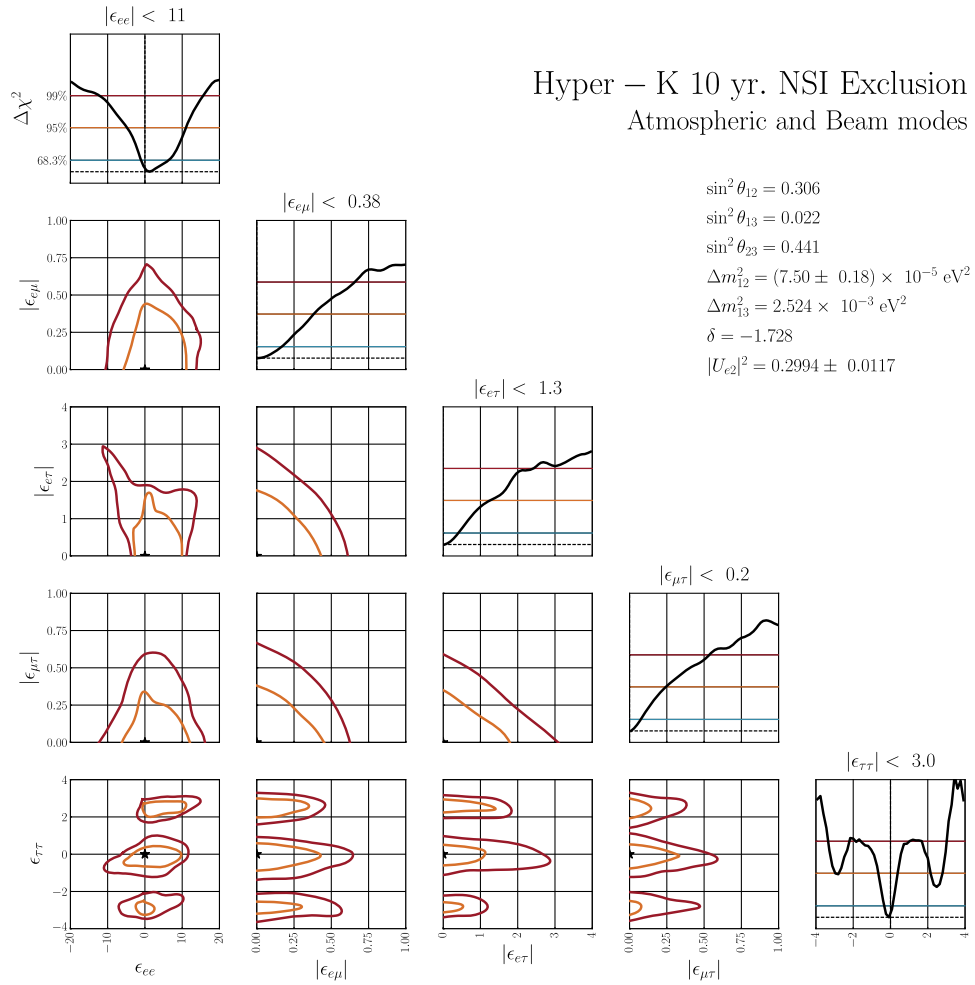

FIG. 7. Expected sensitivity to nonzero NSI assuming ten years of beam- and atmospheric-based data collection at Hyper-Kamiokande at 95% C.L. (orange) and 99% C.L. (red). In each panel, all unseen parameters, including three-neutrino parameters and phases of off diagonal NSI, are marginalized. The top panel of each column displays expected one-dimensional $\Delta\chi^2$ sensitivity for each parameter, including horizontal lines displaying 68.3% (blue), 95% (orange), and 99% (red) C.L. Above each column, the expected limits at 95% C.L. for each parameter are shown. Gaussian priors are included on the values of $|U_{e2}|^2 = 0.2994 \pm 0.0117$ and $\Delta m^2_{12} = (7.50 \pm 0.18) \times 10^{-5}$ eV^2. Estimated sensitivities are calculated utilizing EMCEE [107].

Figure 5 additionally displays results of our analysis incorporating both beam- and atmospheric-based detection (teal). We see small improvement in both the $\sin^2\phi_{24}$—and $4|U_{e4}|^2|U_{\mu4}|^2$—Δm^2_{14} planes; however, it is limited, likely due to the 10% normalization uncertainty included in the atmospheric neutrino sample. The Super-Kamiokande Collaboration noted that oscillations due to sterile neutrinos average out above $\Delta m^2_{14} \gtrsim 10^{-1}$ eV^2 [105], and we see this same behavior in Fig. 5. If a more thorough analysis were performed, particularly including the measurement of electron-type neutrinos in the atmospheric data sample, there would likely be improvement, particularly in the right panel from the sensitivity to two additional oscillation probability channels—$P_{\mu e}$ and P_{ee}.

B. Nonstandard neutrino interactions

Figure 6 displays the expected sensitivity at 95% (orange) and 99% (red) C.L. to nonstandard neutrino interactions assuming ten years of beam-based data collection at Hyper-Kamiokande. In each panel, all unseen parameters (including three-neutrino parameters and phases of complex NSI) are marginalized. At the top of each column, a one dimensional $\Delta\chi^2$ plot is shown for each parameter, including horizontal lines corresponding to 68.3% (blue), 95% (orange), and 99% (red) C.L. We note several degeneracies throughout this figure: most notable are the features in the ϵ_{ee}—$|\epsilon_{e\tau}|$ plane and the degeneracy between $\epsilon_{\tau\tau} = 0$ and $\epsilon_{\tau\tau} \simeq \pm 3$. Degeneracies of this nature have been discussed in the context of long-baseline oscillations in

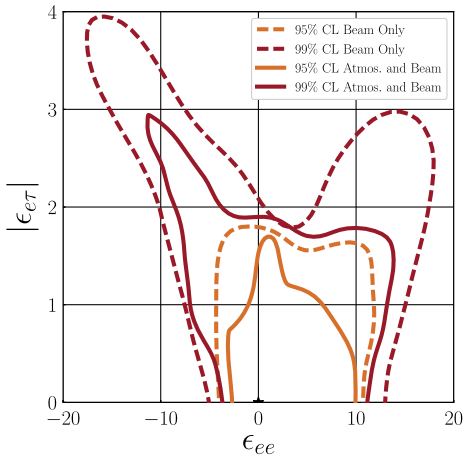

FIG. 8. Improvement in sensitivity to NSI parameters at Hyper-K between considering only beam-based data (dashed lines) and including atmospheric-based data as well (solid lines). Contours shown are 95% C.L. (orange) and 99% C.L. (red) in the ϵ_{ee}—$|\epsilon_{e\tau}|$ plane—all unseen parameters, including the phase on $\epsilon_{e\tau}$ are marginalized. Sensitivities are estimated using EMCEE [107].

Refs. [34,55,62,65,66,73–75,78,81,83,85,92,96]. The $\epsilon_{\tau\tau}$ degeneracy has been discussed at length in Ref. [73], and it arises from a degeneracy between $\epsilon_{\tau\tau}$ and θ_{23} for a nonmaximal physical value of θ_{23} as we have here ($\sin^2\theta_{23} = 0.441$).

Results of the analysis including both beam- and atmospheric-based data are shown in Fig. 7. A direct comparison between this and the results of Super-K [112] and IceCube [61,113] is nontrivial, as our analysis includes all NSI parameters simultaneously, as well as allowing for the off diagonal NSI parameters to be complex and CP violating. Allowing for complex $\epsilon_{\mu\tau}$ has been shown to decrease sensitivity significantly in, e.g., Refs. [34,65,66,73,74]. While there is not drastic improvement between the results in Figs. 6 and 7, we note that there is improvement in the degeneracies seen in the ϵ_{ee}—$|\epsilon_{e\tau}|$ plane as well as in alleviating some of the degeneracy seen for $\epsilon_{\tau\tau}$. For direct comparison of the improvement in the ϵ_{ee}—$|\epsilon_{e\tau}|$ plane, we show both expected sensitivities in Fig. 8.

Comparing the results in Figs. 6 and 7 with those from a multiparameter study at DUNE (see Refs. [73,74]), we see that, even with atmospheric neutrino data, the expected sensitivity reach to NSI at Hyper-K is between a factor of 5 to 10 weaker than that at DUNE. This is unsurprising: NSI effects grow at larger baselines if the same L/E_ν ratio is being probed—the baseline length of Hyper-K (295 km) is significantly shorter than that of DUNE (1300 km). A combined analysis could prove useful—while Hyper-K does not constrain the NSI parameters significantly better than DUNE, the combination of beam- and atmospheric-based data clears up degeneracies that trouble DUNE. With DUNE and Hyper-K data measuring neutrino oscillations in the same range of L/E_ν values and at vastly different baseline lengths, many of these degeneracies may be lifted with a combination of data. Additionally, as noted in the context of sterile neutrinos, the addition of electron neutrino measurements in the atmospheric-based data would aide in improving NSI sensitivity at Hyper-K, particularly in the parameters ϵ_{ee}, $|\epsilon_{e\mu}|$, and $|\epsilon_{e\tau}|$, which are more relevant for oscillation probabilities $P_{\mu e}$ and P_{ee} than for $P_{\mu\mu}$ and $P_{e\mu}$.

V. DISCUSSION AND CONCLUSIONS

Upcoming long-baseline, large-statistics neutrino oscillation experiments such as Hyper-Kamiokande and the Deep Underground Neutrino Experiment will be able to measure the remaining parameters regarding three-neutrino mixing and oscillation, and will additionally start to probe whether the mixing is CP invariant. These upcoming experiments will also have the ability to detect physics beyond the three-massive-neutrinos paradigm. In this work, we explored the capability of Hyper-K to detect two of these new-physics hypotheses: the existence of a fourth, sterile neutrino, and the existence of additional neutrino interactions other than the weak interactions.

We discussed the ways in which these new-physics hypotheses manifest themselves in neutrino oscillations at long baselines, as well as in oscillations of atmospheric neutrinos propagating through the Earth. The latter is important, as the measurement of atmospheric neutrinos is key in the ability of Hyper-K to achieve its physics goals, in addition to the measurement of beam-based neutrinos from J-PARC. The specifics of the beam- and atmospheric-based neutrino capabilities were discussed in some detail, including discussing backgrounds considered in the beam-based measurements.

We performed simulations assuming the Hyper-K detectors will have a total mass of 0.99 megatons (0.56 Mton fiducial), and that the experiment will last ten years. While more recent proposals have suggested placing one of the two Hyper-K detectors in Korea, we considered only the proposal that both are in Japan, 295 km from the origin of the neutrino beam at J-PARC. We have assumed that the beam, capable of running in both neutrino and antineutrino modes, has a ratio of runtime of $1:3$ for $\nu:\bar{\nu}$ modes. Given the size of the detector, we estimate that the total yield of atmospheric neutrinos will be 20 times that of Hyper-K's predecessor, Super-Kamiokande. With conservative estimates on this, zenith angle smearing, and smearing over expected energy, as well as only considering muon-type neutrinos, we calculate the expected yields for low- and high-energy neutrinos at Hyper-K.

The yields we calculate are used, along with conservative estimates for signal and background normalization uncertainties, in a Markov chain Monte Carlo algorithm to calculate expected sensitivities using a chi-squared statistic approach. We presented our results in terms of sensitivity

reach of the Hyper-K experiment at 95% and 99% C.L, showing both the expected reach for beam-based measurements only, and the improvement when atmospheric-based measurements are included as well. We find that Hyper-K is able to reach new regions of parameter space that have yet to be explored by existing experiments, and that it will be competitive with DUNE. The results shown assumed that the neutrino mass hierarchy is discovered prior to Hyper-K collecting data, and that the hierarchy is normal. We also only included muon-type neutrinos in the atmospheric-based data sample: including electron appearance in this sample would improve sensitivity to new physics as well.

We also briefly discussed the complementarity of DUNE and Hyper-K, as the two experiments measure neutrino oscillations in the same range of L/E_ν, the baseline length divided by the neutrino energy; however, they have vastly different values for L and E_ν. This overlap in L/E_ν allows the experiments to probe for new physics phenomena in complementary ways, and a combined analysis between the experiments would be able to better search for these new phenomena.

ACKNOWLEDGMENTS

We would like thank André de Gouvêa and Jeff Berryman for useful discussions regarding this work. This work is supported in part by DOE Grant No. desc0010143. We also acknowledge the use of the Quest computing cluster at Northwestern University for a portion of this research.

[1] K. Abe *et al.* (Hyper-Kamiokande Proto-Collaboration), Physics potential of a long-baseline neutrino oscillation experiment using a J-PARC neutrino beam and Hyper-Kamiokande, Prog. Theor. Exp. Phys. **2015**, 53C02 (2015).

[2] K. Abe *et al.* (Hyper-Kamiokande Proto-Collaboration), Physics potentials with the second Hyper-Kamiokande detector in Korea, arXiv:1611.06118.

[3] C. Adams *et al.* (LBNE Collaboration), The long-baseline neutrino experiment: Exploring fundamental symmetries of the Universe, arXiv:1307.7335.

[4] R. Acciarri *et al.* (DUNE Collaboration), Long-Baseline Neutrino Facility (LBNF) and Deep Underground Neutrino Experiment (DUNE), arXiv:1512.06148.

[5] S. Antusch, C. Biggio, E. Fernandez-Martinez, M. B. Gavela, and J. Lopez-Pavon, Unitarity of the leptonic mixing matrix, J. High Energy Phys. 10 (2006) 084.

[6] X. Qian, C. Zhang, M. Diwan, and P. Vogel, Unitarity tests of the neutrino mixing matrix, arXiv:1308.5700.

[7] S. Parke and M. Ross-Lonergan, Unitarity and the three flavor neutrino mixing matrix, Phys. Rev. D **93**, 113009 (2016).

[8] D. O. Caldwell and R. N. Mohapatra, Neutrino mass explanations of solar and atmospheric neutrino deficits and hot dark matter, Phys. Rev. D **48**, 3259 (1993).

[9] A. Aguilar-Arevalo *et al.* (LSND Collaboration), Evidence for neutrino oscillations from the observation of anti-neutrino(electron) appearance in a anti-neutrino(muon) beam, Phys. Rev. D **64**, 112007 (2001).

[10] A. A. Aguilar-Arevalo *et al.* (MiniBooNE Collaboration), Unexplained Excess of Electronlike Events from a 1-GeV Neutrino Beam, Phys. Rev. Lett. **102**, 101802 (2009).

[11] G. Mention, M. Fechner, T. Lasserre, T. A. Mueller, D. Lhuillier, M. Cribier, and A. Letourneau, The reactor antineutrino anomaly, Phys. Rev. D **83**, 073006 (2011).

[12] D. Frekers *et al.*, The Ga-71(He-3, t) reaction and the low-energy neutrino response, Phys. Lett. B **706**, 134 (2011).

[13] A. A. Aguilar-Arevalo *et al.* (MiniBooNE Collaboration), Improved Search for $\bar{\nu}_\mu \to \bar{\nu}_e$ Oscillations in the MiniBooNE Experiment, Phys. Rev. Lett. **110**, 161801 (2013).

[14] A. A. Aguilar-Arevalo *et al.* (MiniBooNE Collaboration), Improved Search for $\bar{\nu}_\mu \to \bar{\nu}_e$ Oscillations in the MiniBooNE Experiment, Phys. Rev. Lett. **110**, 161801 (2013).

[15] A. de Gouvêa, K. J. Kelly, and A. Kobach, *CP*-invariance violation at short-baseline experiments in $3+1$ neutrino scenarios, Phys. Rev. D **91**, 053005 (2015).

[16] D. Adey, R. Bayes, A. Bross, and P. Snopok, nuSTORM and a path to a muon collider, Annu. Rev. Nucl. Part. Sci. **65**, 145 (2015).

[17] S. Gariazzo, C. Giunti, M. Laveder, Y. F. Li, and E. M. Zavanin, Light sterile neutrinos, J. Phys. G **43**, 033001 (2016).

[18] C. Giunti, Light sterile neutrinos: Status and perspectives, Nucl. Phys. **B908**, 336 (2016).

[19] S. Choubey and D. Pramanik, Constraints on sterile neutrino oscillations using DUNE near detector, Phys. Lett. B **764**, 135 (2017).

[20] A. Donini, M. Maltoni, D. Meloni, P. Migliozzi, and F. Terranova, $3+1$ sterile neutrinos at the CNGS, J. High Energy Phys. 12 (2007) 013.

[21] A. Dighe and S. Ray, Signatures of heavy sterile neutrinos at long baseline experiments, Phys. Rev. D **76**, 113001 (2007).

[22] A. de Gouvêa and T. Wytock, Light sterile neutrino effects at theta(3)-sensitive reactor neutrino experiments, Phys. Rev. D **79**, 073005 (2009).

[23] D. Meloni, J. Tang, and W. Winter, Sterile neutrinos beyond LSND at the neutrino factory, Phys. Rev. D **82**, 093008 (2010).

[24] B. Bhattacharya, A. M. Thalapillil, and C. E. M. Wagner, Implications of sterile neutrinos for medium/long-baseline neutrino experiments and the determination of θ_{13}, Phys. Rev. D **85**, 073004 (2012).

[25] D. Hollander and I. Mocioiu, Minimal $3+2$ sterile neutrino model at LBNE, Phys. Rev. D **91**, 013002 (2015).
[26] J. M. Berryman, A. de Gouvêa, K. J. Kelly, and A. Kobach, Sterile neutrino at the Deep Underground Neutrino Experiment, Phys. Rev. D **92**, 073012 (2015).
[27] Z. Tabrizi and O. L. G. Peres, Hidden interactions of sterile neutrinos as a probe for new physics, Phys. Rev. D **93**, 053003 (2016).
[28] R. Gandhi, B. Kayser, M. Masud, and S. Prakash, The impact of sterile neutrinos on *CP* measurements at long baselines, J. High Energy Phys. 11 (2015) 039.
[29] A. Palazzo, 3-flavor and 4-flavor implications of the latest T2K and NOνA electron (anti-)neutrino appearance results, Phys. Lett. B **757**, 142 (2016).
[30] A. de Gouvêa and A. Kobach, Global constraints on a heavy neutrino, Phys. Rev. D **93**, 033005 (2016).
[31] S. K. Agarwalla, S. S. Chatterjee, A. Dasgupta, and A. Palazzo, Discovery potential of T2K and NOνA in the presence of a light sterile neutrino, J. High Energy Phys. 02 (2016) 111.
[32] S. K. Agarwalla, S. S. Chatterjee, and A. Palazzo, Physics reach of DUNE with a light sterile neutrino, J. High Energy Phys. 09 (2016) 016.
[33] D. Dutta, R. Gandhi, B. Kayser, M. Masud, and S. Prakash, Capabilities of long-baseline experiments in the presence of a sterile neutrino, J. High Energy Phys. 11 (2016) 122.
[34] M. Blennow, P. Coloma, E. Fernandez-Martinez, J. Hernandez-Garcia, and J. Lopez-Pavon, Non-unitarity, sterile neutrinos, and non-standard neutrino interactions, J. High Energy Phys. 04 (2017) 153.
[35] A. Atre, T. Han, S. Pascoli, and B. Zhang, The search for heavy Majorana neutrinos, J. High Energy Phys. 05 (2009) 030.
[36] A. C. Vincent, E. F. Martinez, P. Hernández, M. Lattanzi, and O. Mena, Revisiting cosmological bounds on sterile neutrinos, J. Cosmol. Astropart. Phys. 04 (2015) 006.
[37] M. Drewes and B. Garbrecht, Experimental and cosmological constraints on heavy neutrinos, arXiv:1502.00477.
[38] F. F. Deppisch, P. S. Bhupal Dev, and A. Pilaftsis, Neutrinos and collider physics, New J. Phys. **17**, 075019 (2015).
[39] R. Adhikari *et al.*, A white paper on keV sterile neutrino dark matter, J. Cosmol. Astropart. Phys. 01 (2017) 025.
[40] L. Wolfenstein, Neutrino oscillations in matter, Phys. Rev. D **17**, 2369 (1978).
[41] M. M. Guzzo, A. Masiero, and S. T. Petcov, On the MSW effect with massless neutrinos and no mixing in the vacuum, Phys. Lett. B **260**, 154 (1991).
[42] P. I. Krastev and S. T. Petcov, Recent solar neutrino observations and unconventional neutrino properties, Phys. Lett. B **299**, 99 (1993).
[43] A. Friedland, C. Lunardini, and C. Pena-Garay, Solar neutrinos as probes of neutrino matter interactions, Phys. Lett. B **594**, 347 (2004).
[44] O. G. Miranda, M. A. Tortola, and J. W. F. Valle, Are solar neutrino oscillations robust?, J. High Energy Phys. 10 (2006) 008.
[45] A. Bolanos, O. G. Miranda, A. Palazzo, M. A. Tortola, and J. W. F. Valle, Probing non-standard neutrino-electron interactions with solar and reactor neutrinos, Phys. Rev. D **79**, 113012 (2009).
[46] A. Palazzo and J. W. F. Valle, Confusing non-zero θ_{13} with non-standard interactions in the solar neutrino sector, Phys. Rev. D **80**, 091301 (2009).
[47] F. J. Escrihuela, O. G. Miranda, M. A. Tortola, and J. W. F. Valle, Constraining nonstandard neutrino-quark interactions with solar, reactor and accelerator data, Phys. Rev. D **80**, 105009 (2009); Erratum, Phys. Rev. D **80**, 129908 (2009).
[48] M. C. Gonzalez-Garcia, M. M. Guzzo, P. I. Krastev, H. Nunokawa, O. L. G. Peres, V. Pleitez, J. W. F. Valle, and R. Zukanovich Funchal, Atmospheric Neutrino Observations and Flavor Changing Interactions, Phys. Rev. Lett. **82**, 3202 (1999).
[49] N. Fornengo, M. C. Gonzalez-Garcia, and J. W. F. Valle, On the interpretation of the atmospheric neutrino data in terms of flavor changing neutrino interactions, J. High Energy Phys. 07 (2000) 006.
[50] N. Fornengo, M. Maltoni, R. Tomas, and J. W. F. Valle, Probing neutrino nonstandard interactions with atmospheric neutrino data, Phys. Rev. D **65**, 013010 (2001).
[51] P. Huber and J. W. F. Valle, Nonstandard interactions: Atmospheric versus neutrino factory experiments, Phys. Lett. B **523**, 151 (2001).
[52] A. Friedland, C. Lunardini, and M. Maltoni, Atmospheric neutrinos as probes of neutrino-matter interactions, Phys. Rev. D **70**, 111301 (2004).
[53] A. Friedland and C. Lunardini, A test of tau neutrino interactions with atmospheric neutrinos and K2K, Phys. Rev. D **72**, 053009 (2005).
[54] O. Yasuda, Sensitivity of T2KK to non-standard interactions, Nucl. Phys. B, Proc. Suppl. **217**, 220 (2011).
[55] M. C. Gonzalez-Garcia, M. Maltoni, and J. Salvado, Testing matter effects in propagation of atmospheric and long-baseline neutrinos, J. High Energy Phys. 05 (2011) 075.
[56] A. Esmaili and A. Yu. Smirnov, Probing non-standard interaction of neutrinos with IceCube and DeepCore, J. High Energy Phys. 06 (2013) 026.
[57] S. Choubey and T. Ohlsson, Bounds on non-standard neutrino interactions using PINGU, Phys. Lett. B **739**, 357 (2014).
[58] I. Mocioiu and W. Wright, Non-standard neutrino interactions in the mu-tau sector, Nucl. Phys. **B893**, 376 (2015).
[59] S. Fukasawa and O. Yasuda, Constraints on the nonstandard interaction in propagation from atmospheric neutrinos, Adv. High Energy Phys. **2015**, 820941 (2015).
[60] S. Choubey, A. Ghosh, T. Ohlsson, and D. Tiwari, Neutrino physics with non-standard iinteractions at INO, J. High Energy Phys. 12 (2015) 126.
[61] J. Salvado, O. Mena, S. Palomares-Ruiz, and N. Rius, Non-standard interactions with high-energy atmospheric neutrinos at IceCube, J. High Energy Phys. 01 (2017) 141.
[62] A. Friedland and C. Lunardini, Two modes of searching for new neutrino interactions at MINOS, Phys. Rev. D **74**, 033012 (2006).
[63] M. Blennow, T. Ohlsson, and J. Skrotzki, Effects of non-standard interactions in the MINOS experiment, Phys. Lett. B **660**, 522 (2008).

[64] A. Esteban-Pretel, J. W. F. Valle, and P. Huber, Can OPERA help in constraining neutrino non-standard interactions?, Phys. Lett. B **668**, 197 (2008).
[65] J. Kopp, P. A. N. Machado, and S. J. Parke, Interpretation of MINOS data in terms of non-standard neutrino interactions, Phys. Rev. D **82**, 113002 (2010).
[66] P. Coloma, A. Donini, J. Lopez-Pavon, and H. Minakata, Non-standard interactions at a neutrino factory: Correlations and *CP* violation, J. High Energy Phys. 08 (2011) 036.
[67] A. Friedland and I. M. Shoemaker, Searching for novel neutrino interactions at NOvA and beyond in light of large θ_{13}, arXiv:1207.6642.
[68] J. A. B. Coelho, T. Kafka, W. A. Mann, J. Schneps, and O. Altinok, Constraints for non-standard interaction $\epsilon_{e\tau}V_e$ from ν_e appearance in MINOS and T2K, Phys. Rev. D **86**, 113015 (2012).
[69] P. Adamson *et al.* (MINOS), Search for flavor-changing non-standard neutrino interactions by MINOS, Phys. Rev. D **88**, 072011 (2013).
[70] I. Girardi, D. Meloni, and S. T. Petcov, The Daya Bay and T2K results on $\sin^2 2\theta_{13}$ and non-standard neutrino interactions, Nucl. Phys. **B886**, 31 (2014).
[71] M. Blennow, S. Choubey, T. Ohlsson, and S. K. Raut, Exploring source and detector non-standard neutrino interactions at ESSνSB, J. High Energy Phys. 09 (2015) 096.
[72] M. Masud, A. Chatterjee, and P. Mehta, Probing *CP* violation signal at DUNE in presence of non-standard neutrino interactions, J. Phys. G **43**, 095005 (2016).
[73] A. de Gouvêa and K. J. Kelly, Non-standard neutrino interactions at DUNE, Nucl. Phys. **B908**, 318 (2016).
[74] P. Coloma, Non-standard interactions in propagation at the Deep Underground Neutrino Experiment, J. High Energy Phys. 03 (2016) 016.
[75] J. Liao, D. Marfatia, and K. Whisnant, Degeneracies in long-baseline neutrino experiments from nonstandard interactions, Phys. Rev. D **93**, 093016 (2016).
[76] D. V. Forero and P. Huber, Hints for Leptonic *CP* Violation or New Physics?, Phys. Rev. Lett. **117**, 031801 (2016).
[77] K. Huitu, T. J. Kärkkäinen, J. Maalampi, and S. Vihonen, Constraining the nonstandard interaction parameters in long baseline neutrino experiments, Phys. Rev. D **93**, 053016 (2016).
[78] P. Bakhti and Y. Farzan, *CP*-violation and non-standard interactions at the MOMENT, J. High Energy Phys. 07 (2016) 109.
[79] M. Masud and P. Mehta, Nonstandard interactions spoiling the *CP* violation sensitivity at DUNE and other long baseline experiments, Phys. Rev. D **94**, 013014 (2016).
[80] O. G. Miranda, M. Tortola, and J. W. F. Valle, New Ambiguity in Probing *CP* Violation in Neutrino Oscillations, Phys. Rev. Lett. **117**, 061804 (2016).
[81] P. Coloma and T. Schwetz, Generalized mass ordering degeneracy in neutrino oscillation experiments, Phys. Rev. D **94**, 055005 (2016).
[82] A. N. Khan, Global analysis of the source and detector nonstandard interactions using the short baseline ν-e and $\bar{\nu}$-e scattering data, Phys. Rev. D **93**, 093019 (2016).
[83] A. de Gouvêa and K. J. Kelly, False Signals of *CP*-Invariance Violation at DUNE, arXiv:1605.09376.
[84] M. Masud and P. Mehta, Nonstandard interactions and resolving the ordering of neutrino masses at DUNE and other long baseline experiments, Phys. Rev. D **94**, 053007 (2016).
[85] M. Blennow, S. Choubey, T. Ohlsson, D. Pramanik, and S. K. Raut, A combined study of source, detector and matter non-standard neutrino interactions at DUNE, J. High Energy Phys. 08 (2016) 090.
[86] P. Bakhti and A. N. Khan, Sensitivities to charged-current nonstandard neutrino interactions at DUNE, arXiv:1607.00065.
[87] Y. Farzan and J. Heeck, Neutrinophilic nonstandard interactions, Phys. Rev. D **94**, 053010 (2016).
[88] D. V. Forero and W.-C. Huang, Sizable NSI from the $SU(2)_L$ scalar doublet-singlet mixing and the implications in DUNE, J. High Energy Phys. 03 (2017) 018.
[89] S. Fukasawa, M. Ghosh, and O. Yasuda, Is nonstandard interaction a solution to the three neutrino tensions?, arXiv:1609.04204.
[90] K. N. Deepthi, S. Goswami, and N. Nath, Nonstandard interactions jeopardizing the hierarchy sensitivity of DUNE, arXiv:1612.00784.
[91] S.-F. Ge and A. Yu. Smirnov, Non-standard interactions and the *CP* phase measurements in neutrino oscillations at low energies, J. High Energy Phys. 10 (2016) 138.
[92] S. Fukasawa, M. Ghosh, and O. Yasuda, Sensitivity of the T2HKK experiment to the non-standard interaction, Phys. Rev. D **95**, 055005 (2017).
[93] S. Fukasawa and O. Yasuda, The possibility to observe the non-standard interaction by the Hyperkamiokande atmospheric neutrino experiment, Nucl. Phys. **B914**, 99 (2017).
[94] J. Liao, D. Marfatia, and K. Whisnant, Nonstandard neutrino interactions at DUNE, T2HK and T2HKK, J. High Energy Phys. 01 (2017) 071.
[95] J. Rout, M. Masud, and P. Mehta, Can we probe intrinsic CP/T violation and non-unitarity at long baseline accelerator experiments?, Phys. Rev. D **95**, 075035 (2017).
[96] M. Ghosh and O. Yasuda, Effect of systematics in T2HK, T2HKK and DUNE, arXiv:1702.06482.
[97] C. Patrignani *et al.* (Particle Data Group), Review of particle physics, Chin. Phys. C **40**, 100001 (2016).
[98] A. M. Dziewonski and D. L. Anderson, Preliminary reference earth model, Phys. Earth Planet. Interiors **25**, 297 (1981).
[99] I. Esteban, M. C. Gonzalez-Garcia, M. Maltoni, I. Martinez-Soler, and T. Schwetz, Updated fit to three neutrino mixing: Exploring the accelerator-reactor complementarity, J. High Energy Phys. 01 (2017) 087, NuFIT 3.0 (2016), www.nu-fit.org.
[100] T. Ohlsson, Status of non-standard neutrino interactions, Rep. Prog. Phys. **76**, 044201 (2013).
[101] T. Kikuchi, H. Minakata, and S. Uchinami, Perturbation theory of neutrino oscillation with nonstandard neutrino interactions, J. High Energy Phys. 03 (2009) 114.
[102] C. Biggio, M. Blennow, and E. Fernandez-Martinez, General bounds on non-standard neutrino interactions, J. High Energy Phys. 08 (2009) 090.

[103] M. C. Gonzalez-Garcia and M. Maltoni, Determination of matter potential from global analysis of neutrino oscillation data, J. High Energy Phys. 09 (2013) 152.

[104] J. A. Formaggio and G. P. Zeller, From eV to EeV: Neutrino cross sections across energy scales, Rev. Mod. Phys. **84**, 1307 (2012).

[105] K. Abe *et al.* (Super-Kamiokande Collaboration), Limits on sterile neutrino mixing using atmospheric neutrinos in Super-Kamiokande, Phys. Rev. D **91**, 052019 (2015).

[106] M. Honda, M. Sajjad Athar, T. Kajita, K. Kasahara, and S. Midorikawa, Atmospheric neutrino flux calculation using the NRLMSISE-00 atmospheric model, Phys. Rev. D **92**, 023004 (2015).

[107] D. Foreman-Mackey, D. W. Hogg, D. Lang, and J. Goodman, emcee: The MCMC hammer, Publ. Astron. Soc. Pac. **125**, 306 (2013).

[108] P. Adamson *et al.* (MINOS), Search for Sterile Neutrinos Mixing with Muon Neutrinos in MINOS, Phys. Rev. Lett. **117**, 151803 (2016).

[109] M. G. Aartsen *et al.* (IceCube), Searches for Sterile Neutrinos with the IceCube Detector, Phys. Rev. Lett. **117**, 071801 (2016).

[110] P. Adamson *et al.* (MINOS, Daya Bay), Limits on Active to Sterile Neutrino Oscillations from Disappearance Searches in the MINOS, Daya Bay, and Bugey-3 Experiments, Phys. Rev. Lett. **117**, 151801 (2016); Publisher's Note, Phys. Rev. Lett. **117**, 209901 (2016).

[111] J. Kopp, P. A. N. Machado, M. Maltoni, and T. Schwetz, Sterile neutrino oscillations: The global picture, J. High Energy Phys. 05 (2013) 050.

[112] G. Mitsuka *et al.* (Super-Kamiokande Collaboration), Study of non-standard neutrino interactions with atmospheric neutrino data in Super-Kamiokande I and II, Phys. Rev. D **84**, 113008 (2011).

[113] M. Day (IceCube Collaboration), Non-standard neutrino interactions in IceCube, J. Phys. Conf. Ser. **718**, 062011 (2016).